Swansea University
Prifysgol Abertawe

Cronfa
Setting Research Free

Cronfa - Swansea University Open Access Repository

_____

This is an author produced version of a paper published in :
Materials and Design

_____

Cronfa URL for this paper:
http://cronfa.swan.ac.uk/Record/cronfa23660

_____

Paper:

I, I., Al Amer, A., Laoui, T., Abbas, A., Al-Aqeeli, N., Patel, F., Khraisheh, M., Atieh, M. & Hilal, N. (2016). Fabrication
and antifouling behaviour of a carbon nanotube. *Materials and Design, 89*, 549-558.

http://dx.doi.org/10.1016/j.matdes.2015.10.018

_____

Accepted Manuscript

Fabrication and antifouling behaviour of a carbon nanotube membrane

Ihsanullah, Adnan Al Amer, Tahar Laoui, Aamir Abbas, Nasir Al-Aqeeli, Faheemuddin Patel, Marwan Khraisheh, Muataz Ali Atieh, Nidal Hilal

Please cite this article as: Ihsanullah, Adnan Al Amer, Tahar Laoui, Aamir Abbas, Nasir Al-Aqeeli, Faheemuddin Patel, Marwan Khraisheh, Muataz Ali Atieh, Nidal Hilal, Fabrication and antifouling behaviour of a carbon nanotube membrane, (2015), doi: 10.1016/j.matdes.2015.10.018
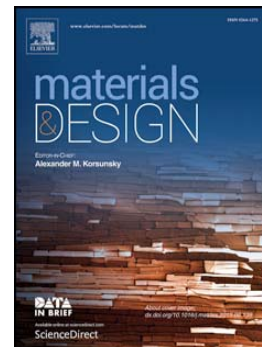
Fabrication and antifouling behaviour of a carbon nanotube membrane

Ihsanullah[1], Adnan Al Amer[1*], Tahar Laoui[2*], Aamir Abbas[1], Nasir Al-Aqeeli[2], Faheemuddin Patel[2], Marwan Khraisheh[3], Muataz Ali Atieh[3&4*], Nidal Hilal[3, 5]

[1]*Department of Chemical Engineering, King Fahd University of Petroleum & Minerals, Dhahran31261, Saudi Arabia*
[2]*Department of Mechanical Engineering, King Fahd University of Petroleum & Minerals, Dhahran 31261, Saudi Arabia*
[3]*Qatar Environment and Energy Research Institute, Qatar Foundation, PO Box 5825, Doha, Qatar*
[4]*College of Science and Engineering, Hamad Bin Khalifa University, Qatar Foundation, PO Box 5825, Doha, Qatar*
[5]*Centre for water Advanced Technologies and Environmental Research (CWATER), College of Engineering, Swansea University, Singleton Park, Swansea SA2 8PP, UK*

*Corresponding authors:
Email: mhussien@qf.org.qa (Muataz A. Hussien)
E-mail: alamer@kfupm.edu.sa (Adnan M. Al Amer)
E-mail: tlaoui@kfupm.edu.sa (Tahar Laoui)

Abstract

In this work, a novel approach is used to synthesize an iron oxide doped carbon nanotube (CNT) membrane, with the goal of fully utilizing the unique properties of CNTs. No binder is used for the synthesis of the membrane; instead, iron oxide particles serve as a binding agent for holding the CNTs together after sintering at high temperature. The produced membrane exhibited a high water flux and strong fouling resistance. In the first step, CNTs were impregnated with various loadings of iron oxide (1, 10, 20, 30 and 50%) via wet chemistry techniques. Impregnated CNTs were then compacted at 200 MPa and sintered at 1350 °C for 5 h to form a compact disk. The membranes were analysed by measuring their porosity, contact angle, diametrical compression test and water flux. The flux of pure water was observed to increase with an increase in iron oxide content. The permeate flux and rejection rate of sodium alginate (SA) were determined to predict the antifouling behavior of the membrane. A maximum removal of 90 and 88% of SA was achieved for membranes with a 10 and 1% iron oxide content, respectively, after 3 h. A minor decline in the permeate flux was observed for all membranes after 4 h of operation.

Keywords: *Membrane, iron oxide, water treatment, carbon nanotubes, S*odium alginate

1. Introduction

Water is the lifeblood of the modern era as a result of the scarcity of resources, drought and expansion of deserts. Reliable access to safe and clean drinking water is considered to be one of the most basic humanitarian goals and remains a major challenge in the 21st century. A report from the United Nations (UN) indicates that 1800 million people will face absolute water scarcity and two-thirds of the world population could be under stress conditions by 2025 [1, 2].

The reuse, recycling and recovery of water has proven to be successful and effective in creating a new and reliable water supply while not compromising public health. Membrane filtration is considered among the most promising and widely used processes for water treatment and desalination [1, 2].

Membranes are classified into different types based on their nominal size or molecular weight cut-off (MWCO), including microfiltration (MF), ultrafiltration (UF), nanofiltration (NF), and reverse osmosis (RO). Microfiltration is employed for suspended solids, protozoa, and bacteria removal; ultrafiltration for virus and colloid removal; nanofiltration for heavy metals dissolved in organic matter and hardness removal; and reverse osmosis for desalination, water reuse, and ultrapure water production [3].

Membranes can also be classified based on their configurations, including hollow fibre, spiral, plate and frame, and tubular. Membranes are manufactured from ceramic, polymeric, or hybrid materials. The most common polymeric membranes are poly(sulfone), poly(amide), poly(propylene), poly(tetrafluoroethylene), cellulose acetate, and poly(vinylidene) fluoride. Most of the ceramic membranes are made using metal oxides including aluminium oxide (Al_2O_3) and titanium oxide (TiO_2), as well as silica (SiO_2), zeolites, microporous carbon, silicon carbide (SiC) and zirconia (ZrO_2). Ceramic membranes are well suited for challenging water purification

3

processes due to their chemical and thermal stabilities. However, ceramic membranes are typically considered too expensive and are recommended only for small scale operations. Polymeric membranes, on the other hand, dominate the current water desalination and purification market because of their excellent mechanical strength under pressure and their high selectivity. However, in many wastewater applications, the current polymeric membranes are less fouling-resistant and chemically stable than ceramic membranes [4].

Typical inorganic membranes are made of ceramic, carbon, silica, zeolite, various oxides and metals. These membranes have been employed in various applications, including gas separation, separation of H_2O from chemical reaction mixtures and the removal of dissolved salts and other contaminants from water. However, these membranes separate the components based on their size [5].

Carbon nanotubes (CNTs) have been rapidly explored among scientists in many fields, including chemistry, physics and material science, owing to their unique properties, such as high aspect ratio, low density, high chemical, thermal, and mechanical strength, and remarkable electrical and optical properties. CNTs have been widely employed for the removal of various contaminants from aqueous solutions. Various experimental studies have reported the adsorption of heavy metal ions [6-13], small molecules like hydrogen and oxygen [14-15] and organic chemicals [17-19] on different CNTs (closed- or open-ended CNTs, single- or multiwalled CNTs).

CNTs have recently attracted considerable attention for the synthesis of novel membranes with attractive features for water purification [20-36]. CNTs can also be used as direct filters and effective fillers to improve the membrane performance. CNTs have proven to be excellent fillers

in membranes due to improved permeability, rejection, disinfection and antifouling behaviour. The flux through CNTs has been estimated to be 3-4 orders of magnitude faster than predicted by the Hagen-Poiseuille equation [22-24].

In recent times, the mixed-matrix membrane has been explored extensively due to its ease of synthesis and broad applications. Various nanoparticles, such as TiO_2 [37-38], Al_2O_3 [39–40], ZrO_2 [41], and SiO_2 [42], can be employed as filler materials for the synthesis of mixed-matrix membranes with improved performance. CNTs are also appealing membrane fillers and act as extraordinary mass transport channels as studied by various research groups. Several studies have shown successful application of CNTs in a polymer matrix [33-35, 43-46]. The addition of CNTs has been reported to substantially increase the water flux due to the hydrophilic surface and large surface pores of the membranes [35]. Moreover, the tensile strength and fouling resistance of the membranes were reported to increase with the addition of CNTs.

The presence of natural organic matter, microorganisms and high concentration of salt in water systems leads to membrane fouling. Typical adverse effects of membrane fouling include (i) a reduction in the membrane water flux, (ii) an increase in the solute concentration polarization, (iii) increased energy requirements; (iv) biodegradation and/or biodeterioration of the membrane materials, (v) an increase in the module differential pressure, and (vi) the establishment of concentrated populations of primary or secondary human pathogens on the membrane [5]. Therefore, fouling is a major obstacle in the widespread application of membrane technology. Several studies have been performed in recent years with the goal of enhancing the fouling resistance of membranes by surface modification with CNTs [5, 47].

This paper describes a novel synthesis concept of a carbon nanotube metal oxide membrane, comprising dispersed CNTs and iron oxide nanoparticles. In the first step, CNTs are impregnated with different amounts of iron oxide (1, 10, 20, 30 and 50%) via a wet chemistry technique. The impregnated CNTs are then compacted and sintered to form a compact disk. The effect of the iron oxide content, compaction force and sintering temperature on the membrane properties was studied. The powder materials were characterized by scanning electron microscopy (SEM), energy dispersive X-ray spectroscopy (EDS), X-ray diffraction (XRD) and thermogravimetric analysis (TGA), while the prepared membranes were analysed by measuring their density, pore size, contact angle measurement and water flux. CNT-iron oxide membranes are expected to efficiently remove heavy metals from water in a continuous flow system. The permeate flux and rejection rate of sodium alginate (SA) were determined to predict the antifouling behaviour of the membrane.

2. Experimental details

2.1. Materials

The carbon nanotubes used in this study were supplied by Chengdu Organic Chemicals Co. Ltd. (China). The CNT specifications are shown in Table 1. Iron (III) nitrate nonahydrate, $Fe(NO_3)_3.9H_2O$ (Reagent grade, Sigma Aldrich, purity $\geq$ 98%) was used as a metal oxide salt for iron oxide.

Table 1

Chemical and physical properties of the carbon nanotubes.

| Property	Value
Outer diameter (nm)	10-30
Length (μm)	1-10
Purity	>95%
Ash	<1.5 weight%
Specific surface area (m^2/g)	> 200
Electrical conductivity (S/cm)	$>10^2$

The iron oxide nanoparticles were impregnated on the surface of CNTs by a wet impregnation method. For example, for a 1% iron oxide loading, 1.443 g of pure ferric nitrate [$Fe(NO_3)_3.9H_2O$] was dissolved in 500 mL of ethanol (98% purity). CNTs (19.88 g) were also dissolved in the 400 mL of absolute ethanol. Both solutions were sonicated for 45 min separately before being mixed together. The resultant mixture was again sonicated for 1 h at room temperature. The aim of ultrasonication is to have complete and homogeneous wetting of the particles during impregnation; this decreases the likelihood of agglomeration, which occurs due to the formation of clumps of liquid. The mixture was then kept in an oven to evaporate the ethanol. The residue was then calcinated for 3.5 h at 350 °C in a furnace to obtain CNTs impregnated with 1% iron oxide. This process leads to homogenously dispersed iron oxide

nanoparticles in a CNT matrix, and the attachment of iron oxide to the CNTs. Similarly, CNTs were doped with different iron oxide loadings, i.e., 10, 20, 30 and 50 %.

3. Characterization

3.1.   SEM, TEM and EDS analysis of raw and impregnated CNTs

Fig. 1 displays the SEM images and EDS spectra of the CNTs and CNT-Fe_2O_3. The presence of the iron oxide particles was confirmed by EDS analysis. High-resolution transmission electron microscopy (HRTEM) was performed to characterize the structure and size of the nanotubes and iron oxide nanoparticles and to observe the configuration adopted by the iron oxide nanoparticles on the surfaces of the CNTs (as shown in Fig. 2). The HRTEM image of the unmodified nanotubes is presented in Fig. 2a. This image shows hollow and tubular nanotubes with an outer diameter of 10-30 nm and an inner diameter of 5-10 nm. Figure 2b shows a typical HRTEM image of CNT-Fe_2O_3 indicating the presence of the iron oxide nanoparticles with an average size of ~3 nm on the surfaces of the CNTs. It was also noted that the structure of the CNTs was not damaged during the nanoparticle impregnation process.
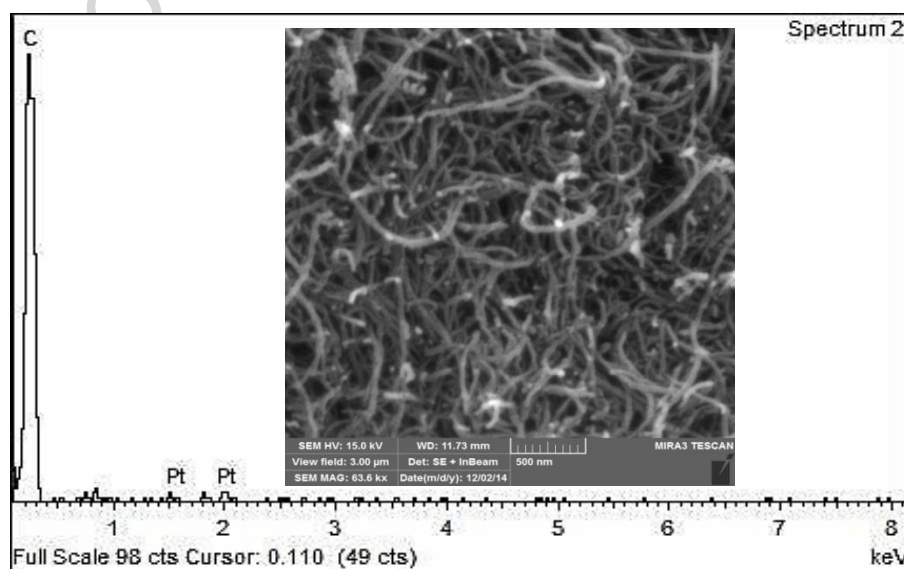
(a) Raw CNTs.
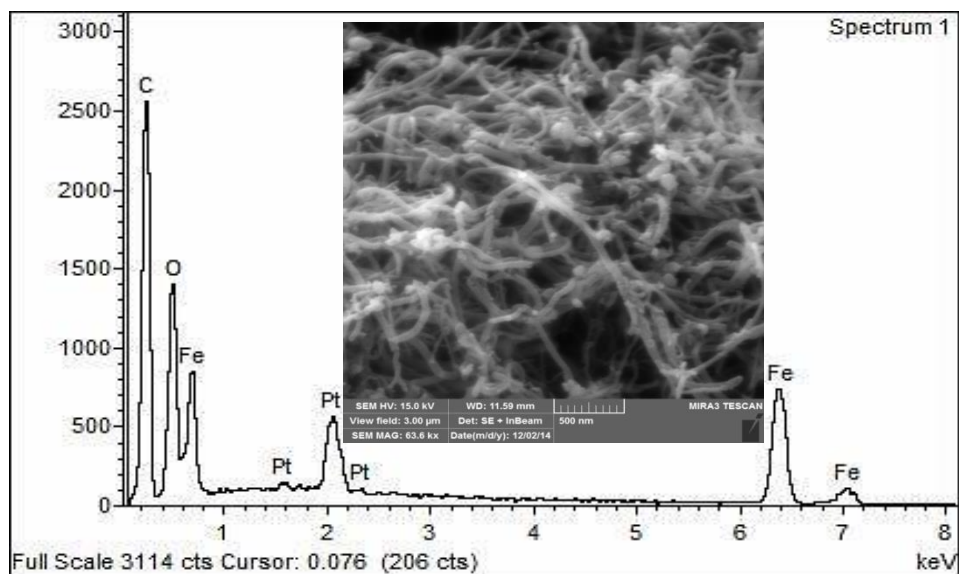
(b) 20 % CNT-Fe$_2$O$_3$.
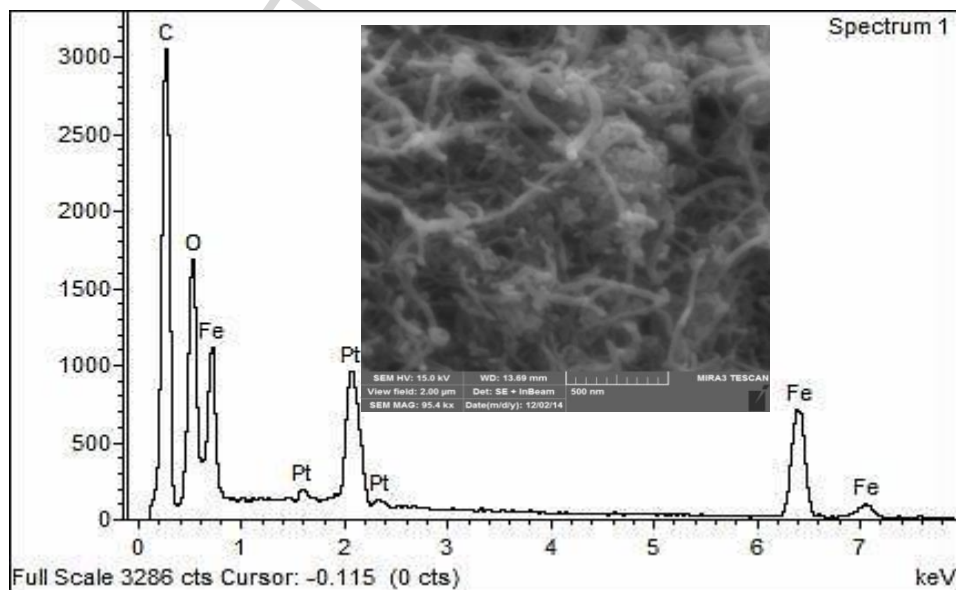
(c) 50 % CNT-Fe$_2$O$_3$.

Fig. 1. SEM and EDS analysis of (a) raw CNTs, (b) 20% CNT-Fe$_2$O$_3$ and (c) 50% CNT-Fe$_2$O$_3$.
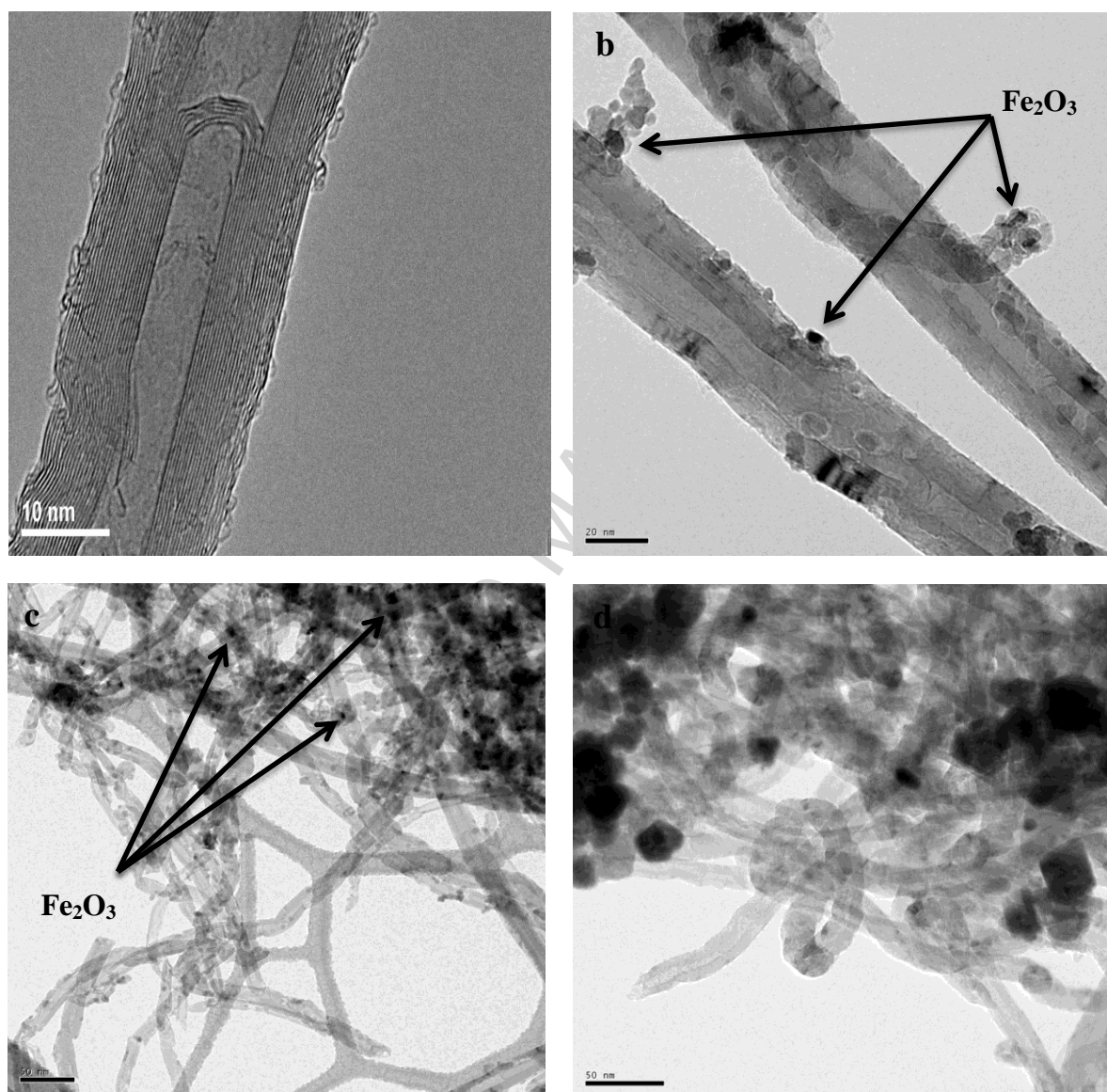
Fig. 2. HRTEM images of (a) raw CNTs and (b, c and d) CNT-Fe$_2$O$_3$.

3.2. *Thermal degradation analysis*

Thermogravimetric analysis (TGA) is an effective technique to evaluate the quality of the CNTs. The metal impurity content associated with the CNTs can be determined by simply burning the CNT samples in air. Fig. 3 displays the TGA curves for the CNTs and CNT-Fe$_2$O$_3$ under air at a

heating rate of 10 °C/min. It was observed that the raw CNTs did not undergo any major mass loss before ~500°C; however, a sharp weight loss was observed thereafter. This weight loss is attributed to the degradation of disordered or amorphous carbon, moisture, ash, and other metal impurities [48-51]. It has also been reported by many researches that amorphous carbon has a low thermal stability due to its lower activation energy for oxidation. The degradation of CNTs at temperatures higher than 500°C corresponds to the thermal oxidation of the remaining disordered carbon [50-51].

For the impregnated CNTs (CNT-Fe_2O_3), the initial oxidation and final oxidation temperatures were observed to decrease. The presence of iron oxide nanoparticles reduced the initial and final degradation temperature of the CNTs by almost 100 °C as shown in Fig.3. The lower thermal stability of the impregnated CNTs when compared to the raw CNTs may be due to the attachment of iron oxide particles to the walls of the CNTs. The lower degradation temperature of iron oxide compared to the raw CNTs leads to the faster degradation of the impregnated CNTs.

TGA was also used to estimate the quantitative loading of Fe_2O_3 onto the CNT surface by weighing the residual matter, which consists of Fe_2O_3 predominantly after the CNTs have been burnt off completely in air. No residual weight was measured after the complete oxidation of raw CNTs; while the weight of CNT samples with 1, 10, 20, 30 and 50% Fe_2O_3 were reduced to 1.2, 11, 22, 32 and 53%, respectively, after being heated at 900°C in air.
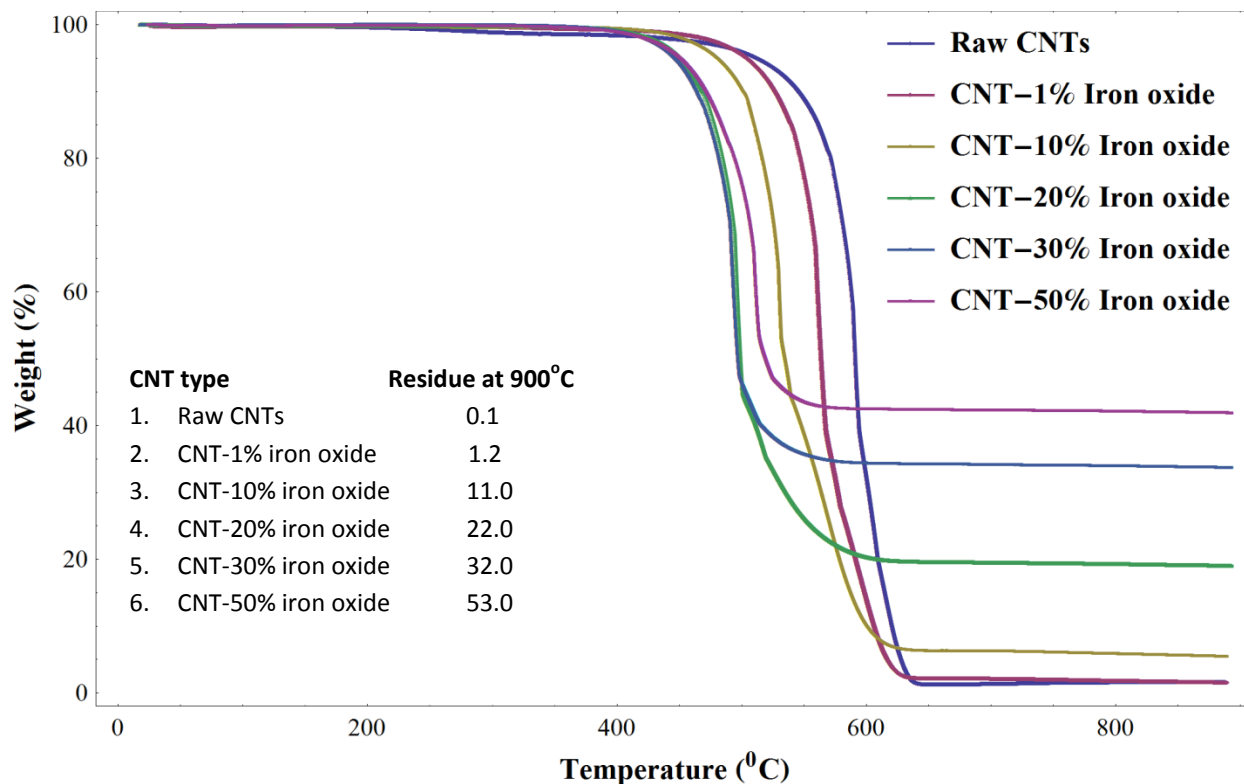
CNT type	Residue at 900°C
1. Raw CNTs	0.1
2. CNT-1% iron oxide	1.2
3. CNT-10% iron oxide	11.0
4. CNT-20% iron oxide	22.0
5. CNT-30% iron oxide	32.0
6. CNT-50% iron oxide	53.0

Fig. 3. Thermogravimetric Analysis (TGA) for raw CNTs and CNT-Fe_2O_3

3.3. X-ray diffraction (XRD)

X-ray diffraction (XRD) of the raw and impregnated CNTs was performed to demonstrate the highly crystalline nature of the composites and confirm the attachment of iron oxide particles to the CNTs. The XRD patterns were recorded using an X-ray diffractometer equipped with a Cu Kα radiation source (40 kV, 20 mA) at a rate of 1.0°/min between 10-80° (2α). Fig. 4 displays the XRD patterns of the raw and doped CNTs. The XRD pattern of the raw CNTs presented two major characteristic peaks at $2\theta \sim 27$ and 44° that correspond to the hexagonal graphite lattice of multi-walled carbon nanotubes. The XRD pattern of the impregnated CNTs presented new peaks in addition to the two obvious peaks associated with carbon nanotubes. The most significant Bragg diffraction peaks observed appeared at $2\theta = 34, 36, 42, 50, 54, 63$ and 65°. These peaks

12

correspond to the α-Fe$_2$O$_3$ nanoparticles [52]. These results demonstrate that the Fe$_2$O$_3$ particles were successfully attached to the CNTs.
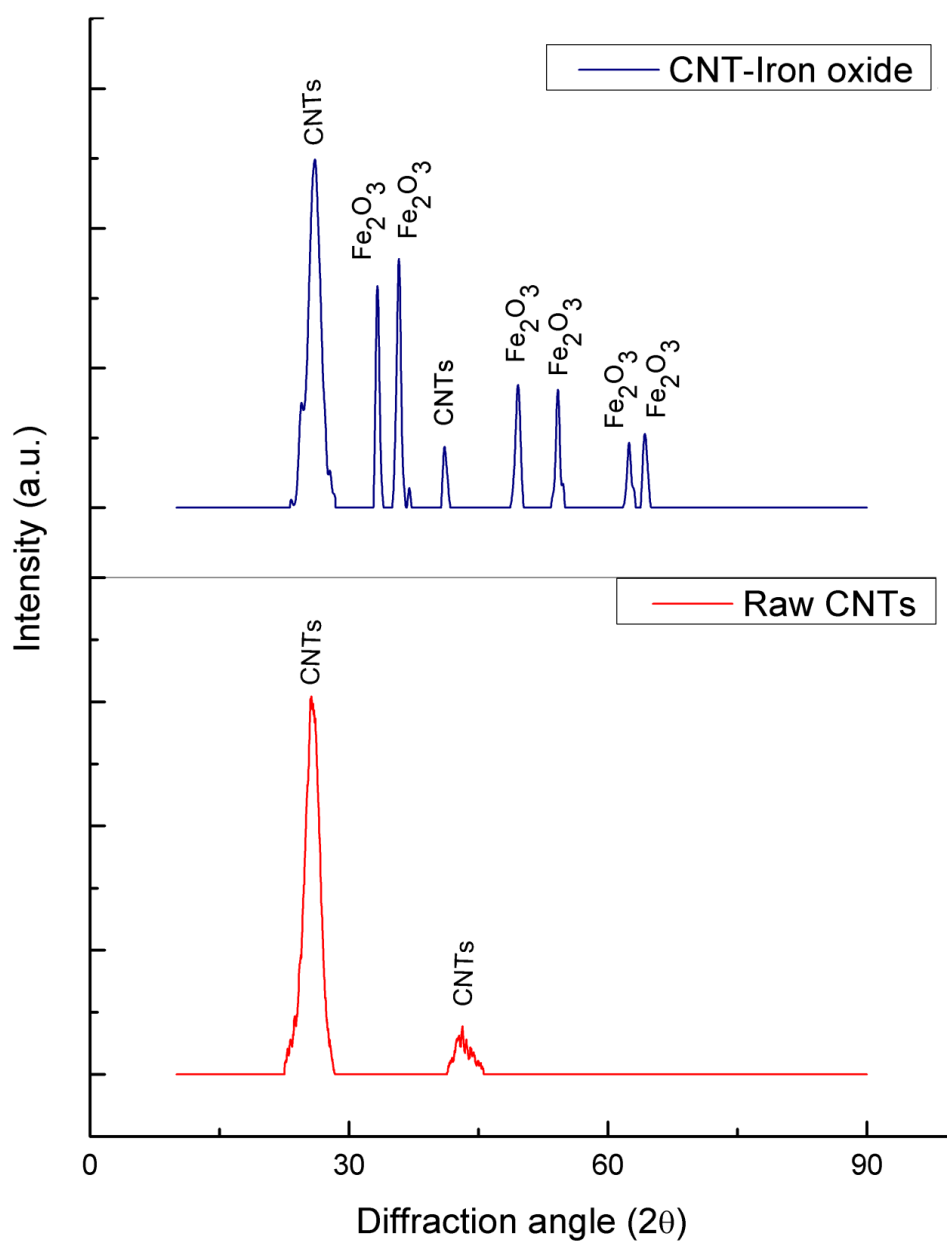

Fig. 4. XRD patterns of the raw CNTs and CNT-Fe$_2$O$_3$.

13

4. Membrane preparation

Carbon nanotube doped iron oxide particles were uniaxially pressed into steel disks with a diameter of 27 mm under a pressure of 200 MPa. Compaction yielded a disk of approximately 27 x 3 mm containing 1, 10, 20, 30 and 50% iron oxide by mass. These disks were sintered in a horizontal tube furnace (MTI Corporation GSL-1700X) with a programmable temperature controller. Sintering was performed at temperature of 1350°C for 5 h under argon gas (300-400 mL/min) at a heating rate of 5°C/min. The membrane characteristics were analysed by SEM, EDS, XRD, porosity and contact angle measurements. A schematic of the membrane synthesis process is presented in Fig. 5.
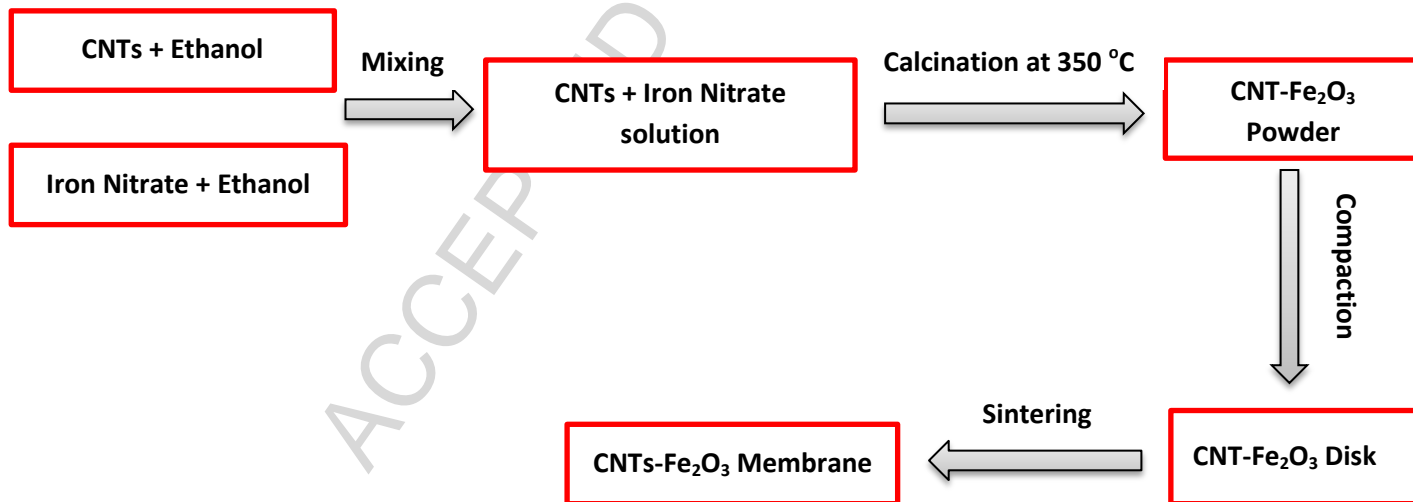

**Fig. 5.** Flow chart of the iron doped CNT membrane synthesis.

4.1. Membrane characterization

4.1.1. Scanning electron microscopy (SEM)

Scanning electron microscopy of the membranes was performed using a field emission scanning electron microscope (TESCAN MIRA 3 FEG-SEM). The membrane samples were sputtered with a 10 nm layer of platinum. Fig. 6 shows the SEM images of the sintered membranes with different iron oxide loadings. It can be seen that the Fe_2O_3 particles are well dispersed at lower particle loadings; however, some aggregation was observed when the amount of Fe_2O_3 loaded was higher. The membrane appears to be more porous, as confirmed by porosity measurements, when the iron oxide content is low. As the Fe_2O_3 loading is increased, the porosity is reduced due to the presence of Fe_2O_3 particles in the channels that exist among the CNTs.
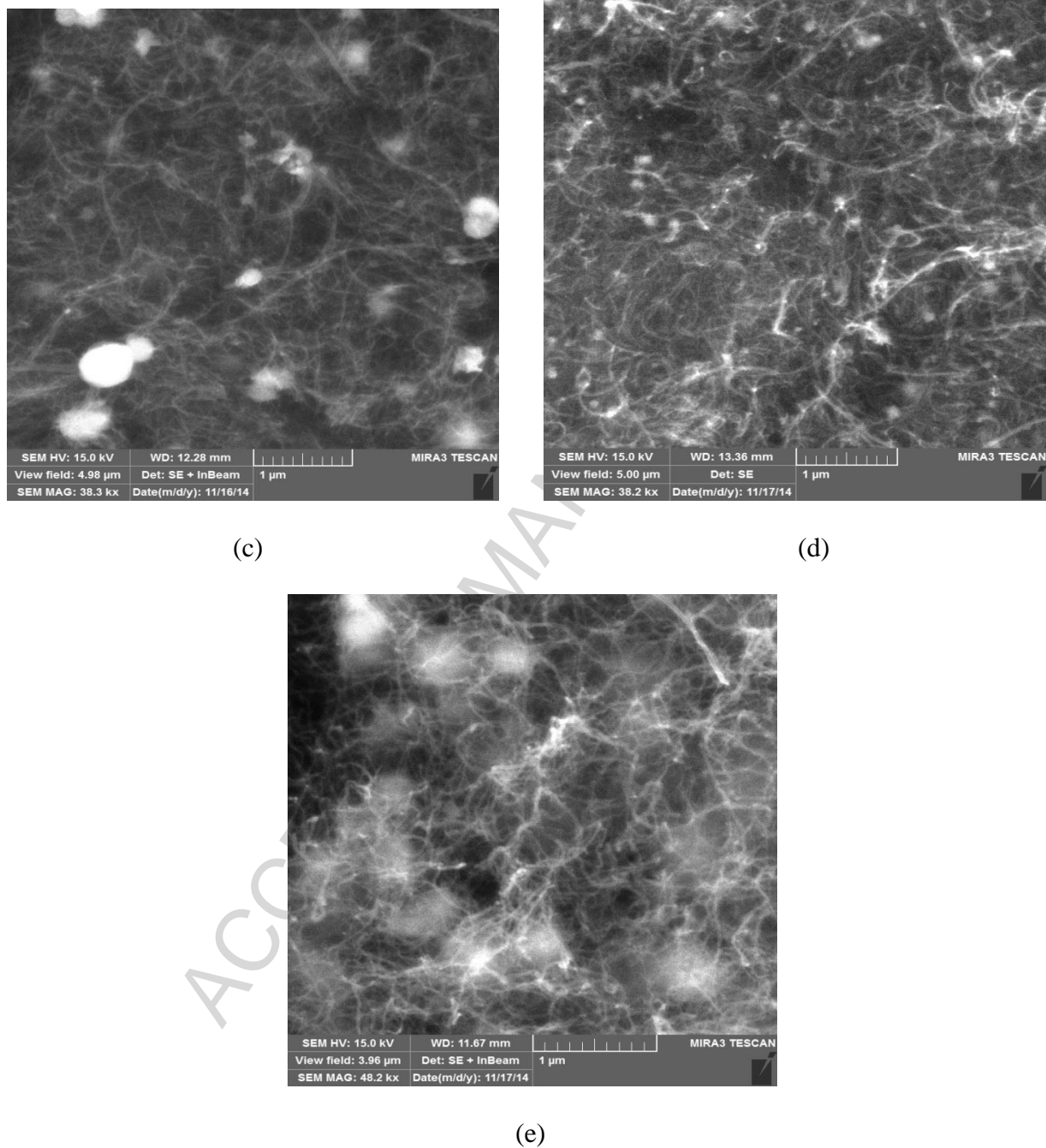

(a)

(b)

(c)

(d)

(e)
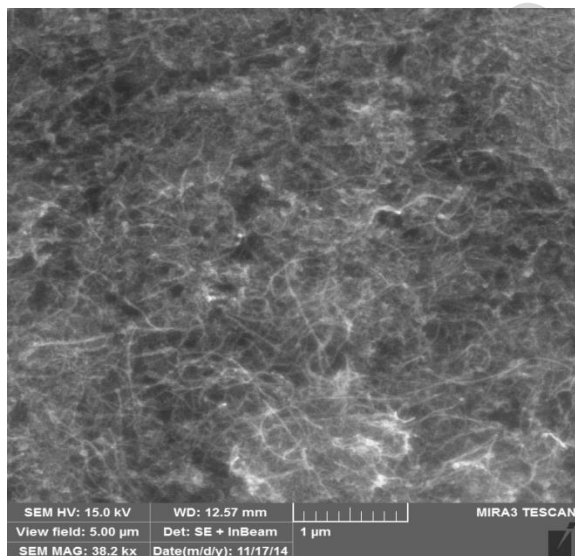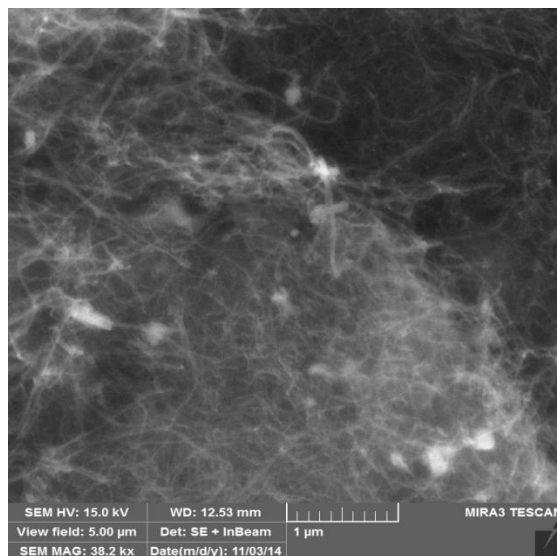
Fig. 6. SEM images of the CNT sintered membranes with (a) 1 (b) 10 (c) 20 (d) 30 and (e) 50% Fe_2O_3.

4.1.2. Porosity measurements

The porosity of the membranes was determined by the dry-wet method [32] using equation (1):

16

$$\text{Porosity} = \frac{W_2 - W_1}{\rho.V} \times 100\ \% \qquad\qquad (1)$$

Where w_1 (g) and w_2 (g) are the weight of the dry and wet membranes, respectively, ρ (g/cm^3) is the density of distilled water at room temperature, V (cm^3) is the volume of the membrane. The weight of the wet membrane was measured after being immersed in distilled water for 24 h. The wet membrane was then dried in an oven at 90 °C for 24 h before measuring its dry weight. In order to minimize the experimental error, the experiment was repeated three times and the average value is reported in Fig. 7.

The porosity of the membrane changes slightly as the iron oxide content is increased from 1 to 10%. However, a decrease in porosity was observed by increasing the iron oxide content from 10 to 30%. This may arise because as the iron oxide content is increased, the space between the CNTs becomes filled with the iron oxide particles, which attach to the CNTs, resulting in the porosity being reduced. After sintering, the particles attached to the CNT walls aggregate to hold the CNTs, and it is expected that the iron oxide particles will exist within the gaps between the CNTs. This leads to a reduction in porosity. Similar behaviour has been reported in the literature, whereby a decrease in flux is observed with filler loading [32, 53].

 However, at higher iron oxide concentrations, the porosity again increases. This may be due to the formation of gaps at relatively high iron oxide loadings (50%) resulting from the agglomeration of iron oxide particles; these gaps allow water molecules to pass through the membrane easily. A similar increase in porosity and flux at a high filler loading is also reported in the literature [54].

However, the change in porosity of the membrane observed by varying the iron oxide loading is very small. This indicates that the iron oxide content is not responsible for the significant change in the membrane porosity observed. The porosity depends predominantly on the CNT properties.
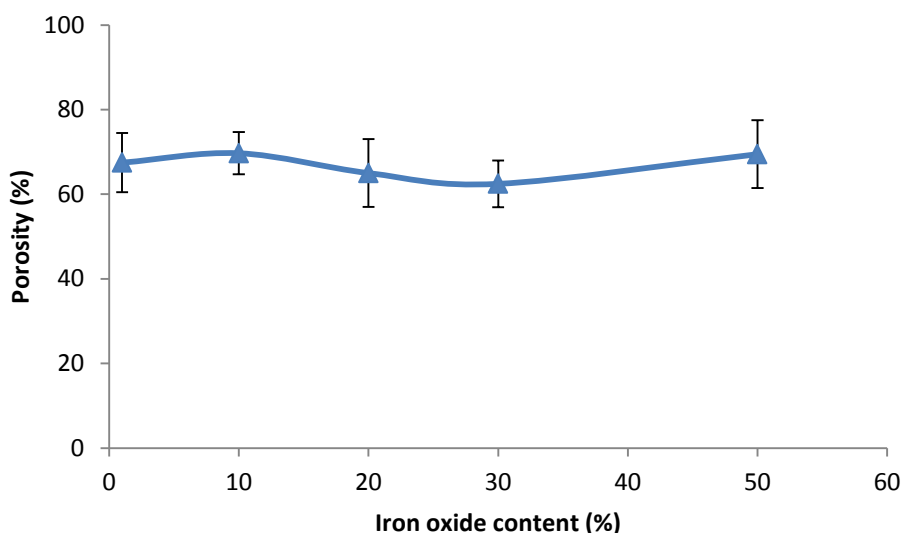

Fig. 7. The varying membrane porosity with Fe_2O_3 content.

4.1.3. Contact angle measurements

The contact angle gives an indication of the hydrophilicity and/or hydrophobicity of the membrane. The contact angle of the membrane surface was measured using a contact angle analyser (KYOWA, model DM-301). The measurements were carried out by placing a 5 µL water droplet onto the membrane surface. All experiments were repeated at five different sites, and the mean value reported.

It can be seen from Fig. 8 and 9 that the contact angle decreases with an increase in the iron oxide content in the membrane. This behaviour indicates that the hydrophilicity of the membrane increases as the iron oxide content increases. The hydrophilic nature of the membrane facilitates

18

the rapid transport of water molecules through it, which results in the enhanced flux observed
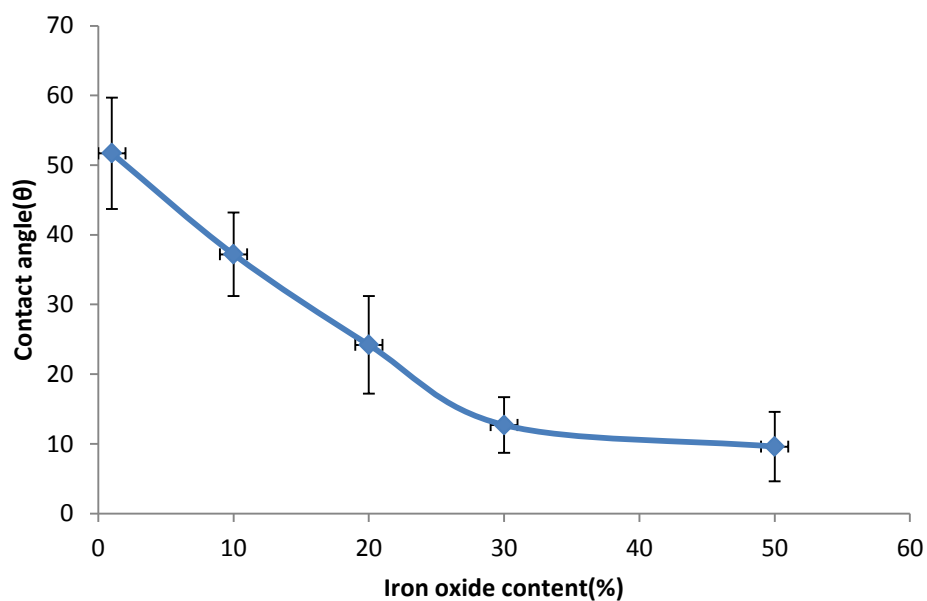[24].

Fig. 8. Contact angle of the membrane versus the iron oxide content.

(a) 1%

(b) 10%

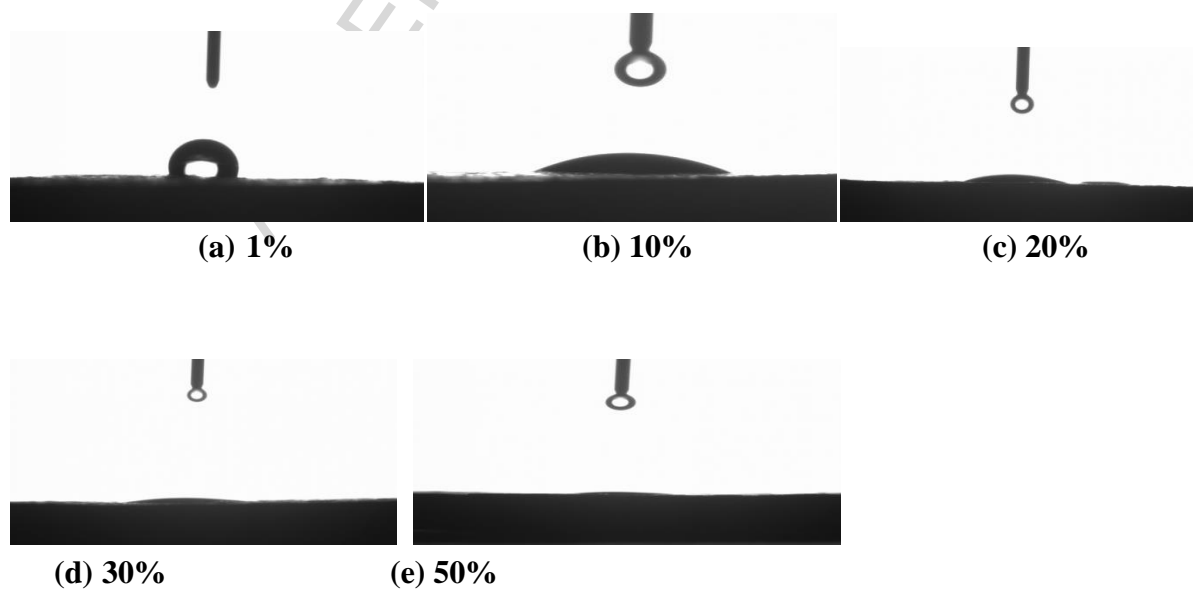**(c) 20%**

(d) 30%

(e) 50%

19

Fig. 9. Contact angle measurement of the membrane with a (a) 1, (b) 10, (c) 20, (d) 30 and (e) 50% iron oxide content.

4.1.4. Diametral compression test

The mechanical strength of the CNT-Fe$_2$O$_3$ membranes was measured by applying the diametral compression test. The diametral compression test is often employed to predict the strength of porous materials. The membranes were pressed diametrally between two flat plates and the tensile strength of the sample was measured in the direction perpendicular to the load. The diametral stress (σ) can be calculated using equation (2) [55-56]:

$$\sigma = 2P/\pi D t \qquad (2)$$

Where *t* and *D* are the thickness and diameter of the membrane disk, respectively, and *P* is the load.

A schematic of the diametral compression is shown in Fig. 10 (a). The membrane samples had a 27 mm diameter and were 3 mm thick as shown in Fig. 10 (b). Samples were diametrally pressed between flat platens in an Instron universal testing machine with a crosshead speed of 0.01 mm/min. A fractured sample is shown in Fig. 10 (c). It can be observed that the sample fractured into two halves, which indicates that the sample underwent a tensile failure [55-56].
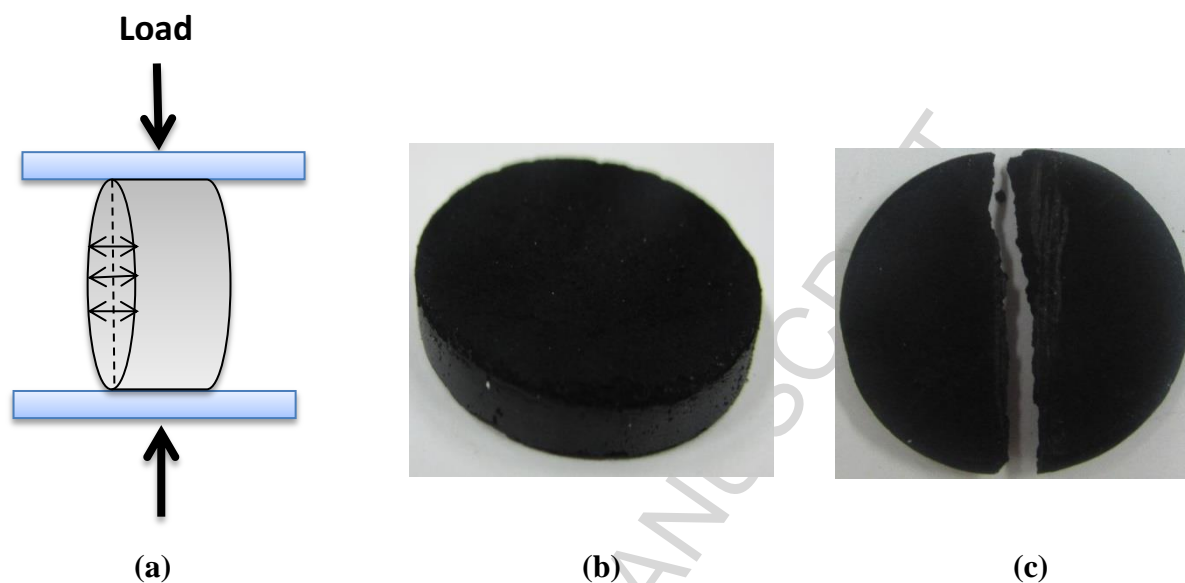
Load

(a)　　　　　　(b)　　　　　　(c)

Fig. 10. (a) Schematic of the diametral compression test and images of the CNT-Fe_2O_3 membrane (b) before and (c) after being subjected to a diametral compression test.

Fig. 11 shows the variation of compressive stress versus compressive strain. It was observed that the maximum compressive strength increases as the silver content in the membrane is increased up to 20% silver loading. This can be justified due to the improved dispersion of iron oxide particles that hold the CNTs together. As a result, the mechanical strength of the membrane increased. A maximum strength of 11.2 MPa was observed for the sample with a 20% Fe_2O_3 content. It was observed that the mechanical strength of the membrane decreases with any further increase in the amount of Fe_2O_3 beyond 20%. This may be due to the agglomeration of iron oxide particles in the matrix, which leads to an increase in porosity. This increase in porosity resulted in a reduction of the mechanical strength of the membrane. Similar reductions in the mechanical strength associated with increased porosity at high filler loadings have been reported [57-58].
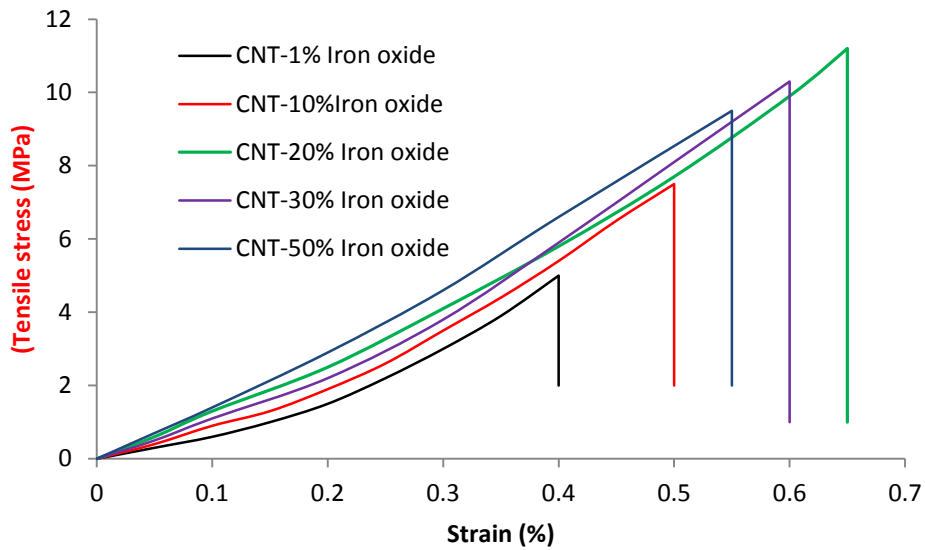
Fig. 11. Diametral compression test curves.

4.2. Water flux measurements

Water transport through the membrane depends predominantly on the hydrophilicity and porosity of the membrane. In general, the flux is higher for hydrophilic membrane surfaces with a high porosity. Water flux measurements were performed using a flow loop system as shown in Fig. 12. The pure water flux was determined by Eq. (3):

$$J = V/A.t \qquad (3)$$

where J $(L.m^{-2}.h^{-1})$ is the pure water flux, V (L) is the volume of permeate water, A (m^2) is the effective area of the membrane and t(h) is the time required for the permeate water to pass through the membrane (h). In our experiments, the surface area of the membrane was 1.4×10^{-3} m^2.
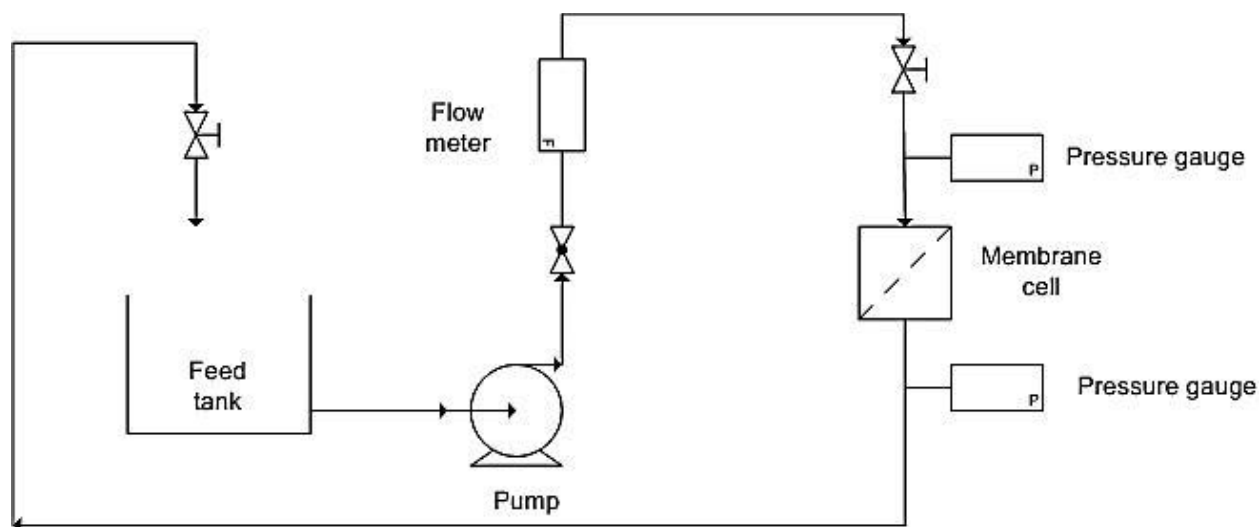
22

Fig. 12. Schematic diagram of the flow loop system.

The pure water flux was measured under different conditions as shown in Fig. 13 and 14. Initially, the water flux was measured at different transmembrane pressures, i.e., from 1 to 40 psi. Then the transmembrane pressure was maintained at 14 psi for 30 min and the water flux was measured. The same procedure was used to obtain the flux at different pressures. Each pressure was maintained for 10 min before recording a reading.

It can be seen from Fig. 13 that the flux increases as the iron oxide content increases. The higher flux of membranes with higher iron oxide concentrations can be justified on the basis of two mechanisms. First, at higher iron oxide content, the membrane surface is more hydrophilic, as confirmed by contact angle measurements. This leads to improved water transport through the membrane. Second, due to the aggregation of iron oxide particles at higher loading, large pores are formed among the CNTs and iron oxide particles; this facilitates a higher flux through the membrane. A slight reduction in the flux was observed with time for all membranes, as shown in Fig, 14. This may be due to the compaction of pores after water flow for long periods of time.
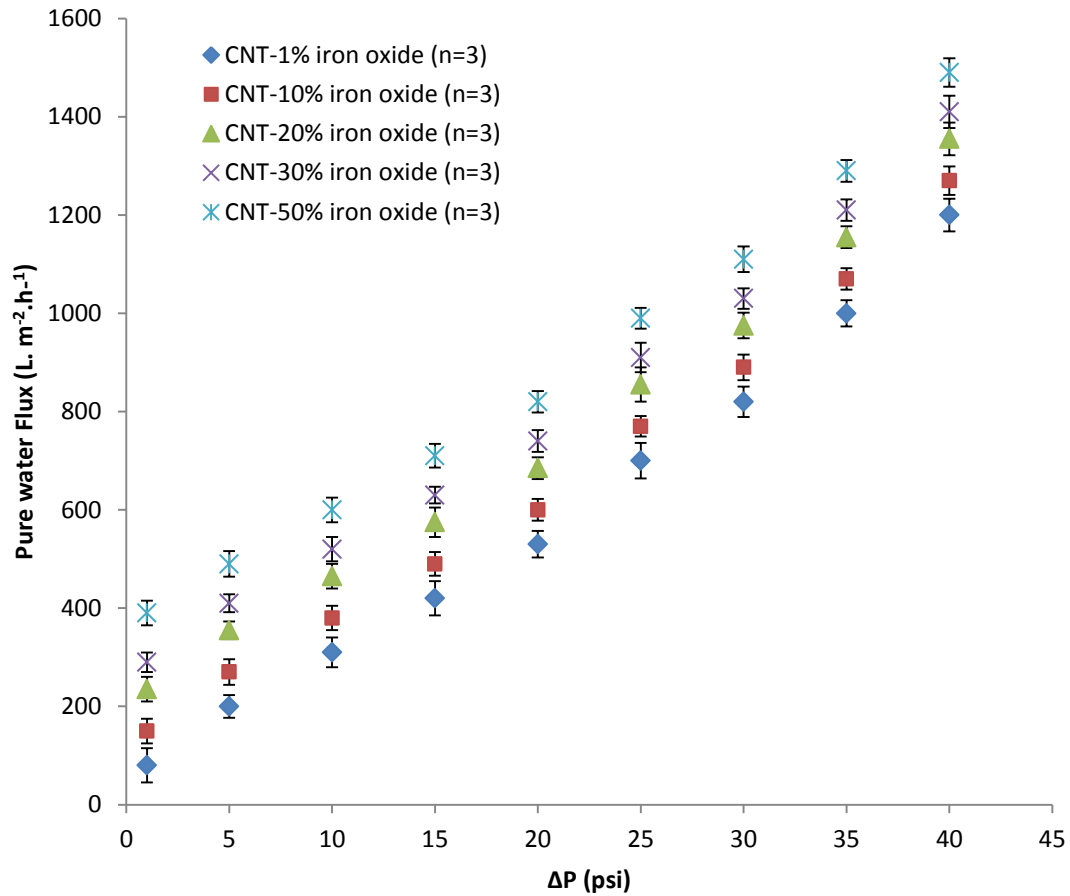
Fig. 13. Effect of transmembrane pressure and iron oxide loading on pure water flux.
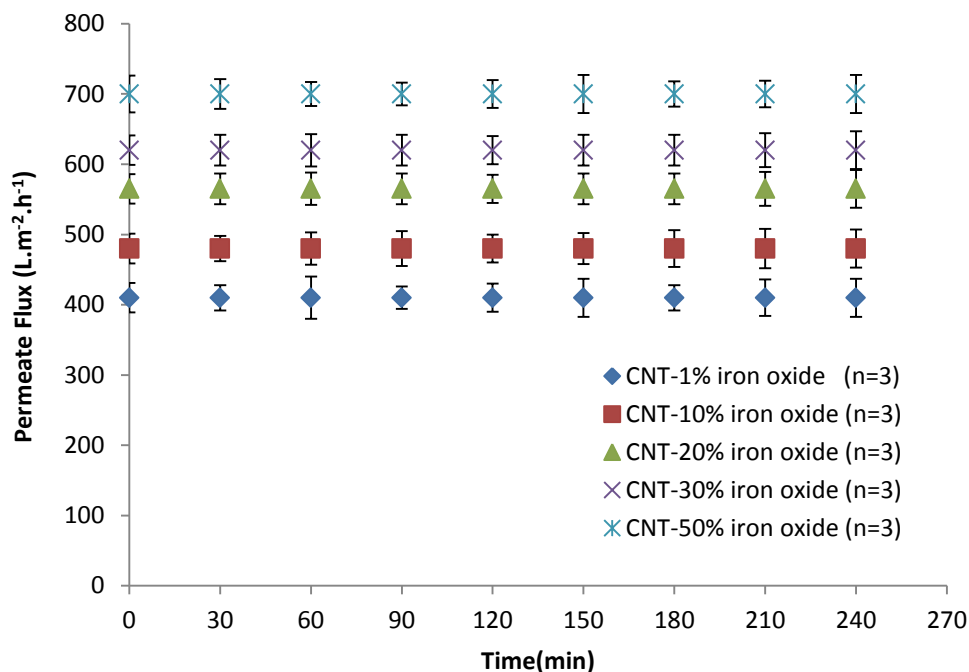
Fig. 14. Effect of time on the pure water flux.

4.3. *Membrane antifouling properties*

Extracellular polymeric substances (EPS) are one of the main causes of membrane fouling in water purification systems. Polysaccharides are major constituents in EPS, while sodium alginate is often used as a model for EPS [59-60].

The permeate flux and rejection rate of sodium alginate (SA) were determined to predict the antifouling behaviour of the membrane. A commercial sodium alginate with a reported molecular weight of 12–80 kDa was supplied by Sigma–Aldrich and employed in all experiments reported here. Alginate solutions with a concentration of 10 ppm were employed in each experiment; the concentration was measured using a total organic carbon (TOC) Shimadzu 5000 A analyser. The ionic strength of the solution was adjusted by the addition of 20 mM NaCl and the pH was maintained at 7.8 by the addition of 1 mM $NaHCO_3$ buffer solution, as reported in the literature [61-63].

Alginate solutions were pumped through the flow loop system at a constant pressure of 14.7 psi, while permeated flux and concentrations were measured after equal time intervals. Results of the analysis are shown in Fig. 15 and 16. It can be observed from Fig. 15 that the permeate flux showed a minor decline after 90 min of operation. The maximum flux remained higher for membranes with an iron oxide content of 50%. This minor decline may be due to the smaller size of alginate, which may pass through the membrane pores with no significant effect on the flux. This suggests that at the initial stage of filtration, adsorption is the main phenomenon that explains the membrane fouling by alginate molecules. After a certain contact time (approximately 90 min in our case), cake development takes place on the membrane surface, which may cause a slight reduction in the permeate flux.

Sodium alginate rejection by the membrane was not significant until 0.5 h of operation, as shown in Fig. 15. This may be due to the smaller molecular size of alginate that requires sufficient time to deposit on the membrane surface and inside the pores. However, the rejection was observed to increase for all membrane types with time afterwards. A maximum rejection of sodium alginate of 90 and 88% was observed for membranes containing 10 and 1% iron oxide, respectively. This result is not surprising since the flux through membranes with low iron oxide content is smaller; hence, the longer contact time between the alginate molecules and membrane surface showed improved adsorption. Furthermore, a relatively good dispersion of iron oxide and CNTs in these membranes contributes to the higher rejection of SA. The membrane with 50% iron oxide was still able to remove 57% alginate molecules after 3 h of operation.
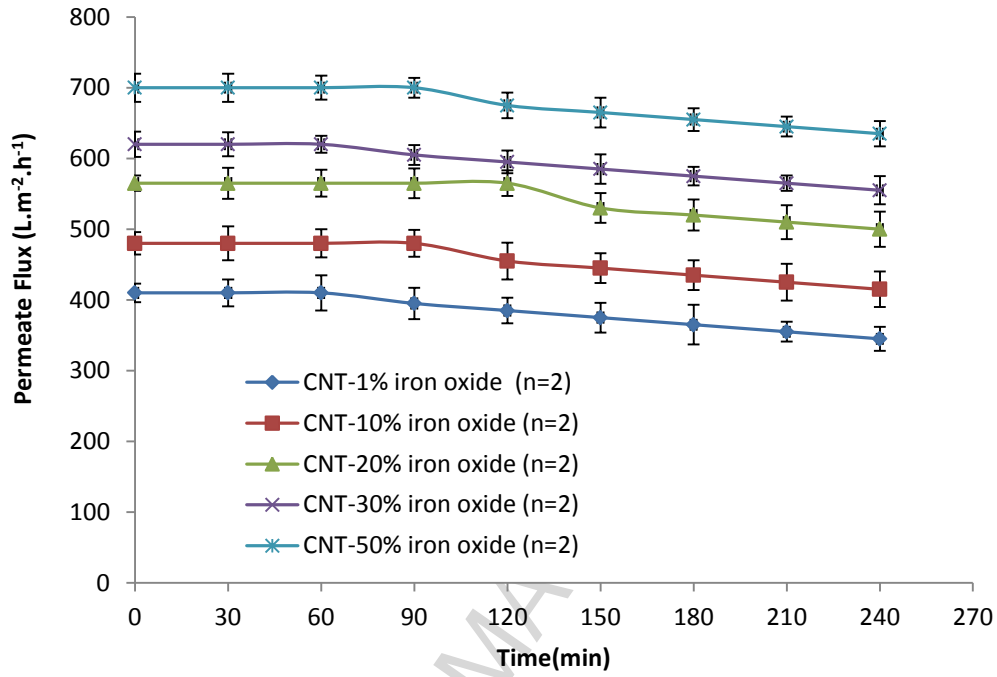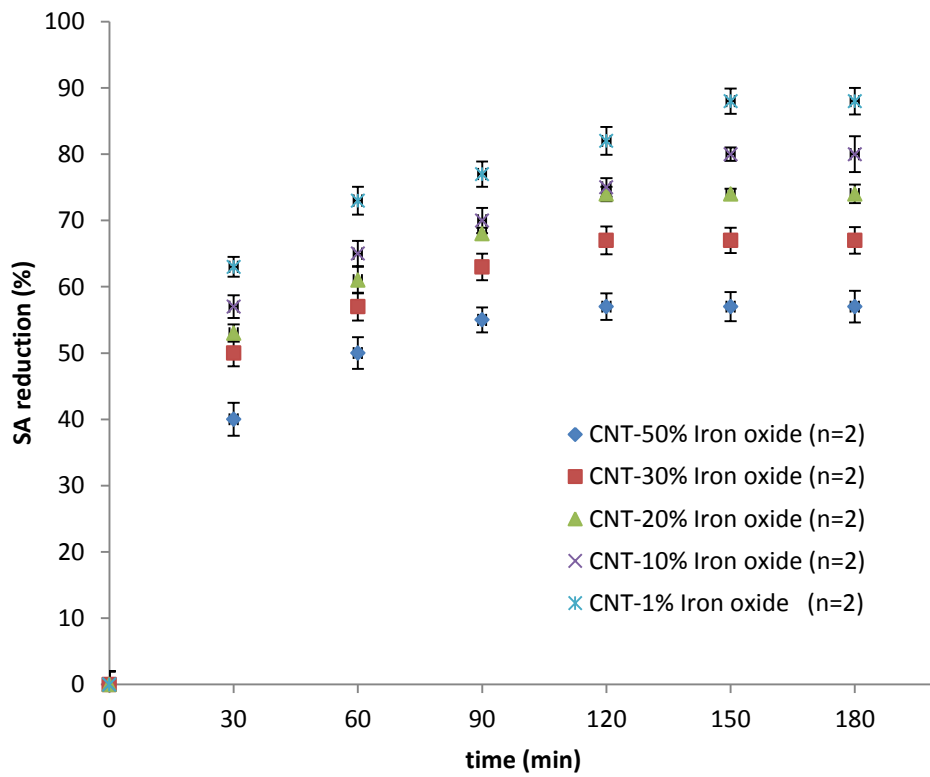
Fig. 15. Permeate flux versus time.

Fig. 16. SA rejection versus time.

27

5.   Conclusions

Iron oxide-doped carbon nanotube membranes were successfully synthesized using a novel approach. The loading of iron oxide in the membrane was varied from 1 to 50 weight%. The produced membrane exhibited a high water flux and strong fouling resistance. The membrane characteristics were influenced remarkably by the iron oxide loading. The flux of pure water was observed to increase as the iron oxide content increased. A maximum flux of 1490 $L.m^{-2}.h^{-1}$ was observed for the membrane with a 50% iron oxide content. As the loading of iron oxide increased, it transformed the membrane from hydrophobic to hydrophilic, as confirmed by contact angle measurements. In addition, the membranes produced displayed a high mechanical strength. A maximum tensile strength of 11.2 MPa was observed for the membrane containing 20% iron oxide. Irrespective of the iron oxide loading, all membranes prepared were effective in removing the SA from water. However, a maximum removal of 90 and 88% of SA was achieved for membranes with a 10 and 1% iron oxide content, respectively, after 3 h. A negligible reduction in the permeate flux was observed with time for all membranes.

References

[1] X. Qu, P.J.J. Alvarez, Q. Li, Applications of nanotechnology in water and wastewater treatment, Water Res. 47 (2013) 3931–3946.

[2] S. Kar, R.C. Bindal, P.K. Tewari, Carbon nanotube membranes for desalination and water purification: Challenges and opportunities, Nano Today 7 (2012) 385-389.

[3] M. Cheryan. Ultrafiltration and Microfiltration Handbook. 2nd ed. CRC Press, 1998.

[4] M.M. Pendergast, E.M.V. Hoek. A review of water treatment membrane nanotechnologies, Energy Environ. Sci. 4 (2011) 1946-1971.

[5] R. Mallada, M. Menéndez, Inorganic Membranes: Synthesis, Characterization and

Applications, 1st ed. Oxford: Elsevier, 2008.

[6] Y.H. Li, J. Ding, Z. Luan, Z. Di, Y. Zhu, C. Xu, D. Wu, B. Wei, Competitive adsorption of Pb^{2+}, Cu^{2+} and Cd^{2+} ions from aqueous solutions by multiwalled carbon nanotubes, Carbon 4 (2003) 2787–2792.

[7] Ihsanullah, F. A. A. Khaldi, B. Abusharkh, M. Khaled, M.A. Atieh, M.S. Nasser, T. laoui, S. Agarwal, I. Tyagi, V. K. Gupta, Adsorptive removal of Cadmium (II) ions from liquid phase using acid modified carbon-based adsorbents, J. Mol. Liq. 204 (2015) 248-254.

[8] Ihsanullah, F. A. A. Khaldi, B. A. Sharkh, A. M. Abulkibash, M. I. Qureshi, T. Laoui, M. A. Atieh, Effect of acid modification on adsorption of hexavalent chromium (Cr(VI)) from aqueous solution by activated carbon and carbon nanotubes, Desalin. water treat. (2015). doi: 1 0.1080/19443994.2015.1021847.

[9] C. Chen, J. Hu, D. Shao, J. Li, X. Wang, Adsorption behavior of multiwall carbon

nanotube/iron oxide magnetic composites for Ni(II) and Sr(II), J. Hazard. Mater. 164 (2009) 923–928.

[10] Z.C.Di, Y.H. Li, Z.K. Laun, J. Liang, Adsorption of chromium(VI) ions from water by carbon nanotubes, Adsorpt. Sci. Technol. 22 (2004) 467–474.

[11] S.G.Wang, W.X. Gong, X.W. Liu, Y.W. Yao, B.Y. Gao, Q.Y. Yue, Removal of lead(II) from aqueous solution by adsorption onto manganese oxide-coated carbon nanotubes, Sep. Purif. Technol. 58 (2007) 17–23.

[12] C. Chen, X. Wang X, Adsorption of Ni(II) from aqueous solution using oxidized multiwall

carbon nanotubes, Ind. Eng. Chem. Res. 45 (2006) 9144–9149.

[13] C.L. Chen, X.K. Wang, M. Nagatsu, Europium adsorption on multiwall carbon nanotube/iron oxide magnetic composite in the presence of polyacrylic acid, Environ. Sci. Technol. 43 (2009) 2362–2367.

[14] C.H. Chen, C.C. Huang, Hydrogen adsorption in defective carbon nanotubes, Sep. Purif. Technol. 65 (2009) 305–310.

[15] A. Gaur, M. Shim, Substrate-enhanced O_2 adsorption and complexity in the Raman G-band spectra of individual metallic carbon nanotubes, Phys. Rev. B. 78 (2008) 1254221-1254227.

[16] J. Goering, E. Kadossov, U. Burghaus, Adsorption kinetics of alcohols on single-wall carbon nanotubes: an ultrahigh vacuum surface chemistry study, J. Phys. Chem. C. 112 (2008) 10114–10124.

[17] H. Hyung, J.H. Kim, Natural organic matter (NOM) adsorption to multi-walled carbon nanotubes: effect of NOM characteristics and water quality parameters, Environ. Sci. Technol. 42 (2008) 4416–4421.

[18] Ihsanullah, H.A. Asmaly, T.A. Saleh, T. Laoui, V.K. Gupta, M.A. Atieh, Enhanced adsorption of phenols from liquids by aluminum oxide/carbon nanotubes: Comprehensive study from synthesis to surface properties, J. Mol. Liq. 206 (2015) 176-182.

[19] H. A. Asmaly, B. Abussaud, Ihsanullah, T. A. Saleh, V. K. Gupta, M. A. Atieh, Ferric Oxide Nanoparticles decorated Carbon nanotubes and carbon nanofibers: from synthesis to Enhanced Removal of Phenol, J. Saudi Chem. Soc. 19 (2015) 511-520.

[20] B.S. Lalia, F. E. Ahmed, T. Shah, N. Hilal, R. Hashaikeh, Electrically conductive membranes based on carbon nanostructures for self-cleaning of biofouling, Desalination 360 (2015) 8–12.

[21] J.K. Holt, A. Noy, T. Huser, D. Eaglesham, O. Bakajin, Fabrication of a carbon Nanotube-cmbedded silicon nitride membrane for studies of nanometer-scale mass transport, Nano Lett. 4 (2004) 2245-2250.

[22] S.Li, G. Liao, Z. Liu, Y. Pan, Q. Wu, Y. Weng, X. Zhang ,Z. Yang, O.K.C. Tsuid, Enhanced water flux in vertically aligned carbon nanotube arrays and polyethersulfone composite membranes, J. Mater. Chem. A. 2 (2014) 12171-12176.

[23] M. Majumder, N. Chopra, R. Andrews, B.J. Hinds, Nanoscale hydrodynamics: Enhanced

flow in carbon nanotubes, Nature 438 (2005) 44-44.

[24] J.K. Holt, H.G. Park, Y. Wang, M. Stadermann, A.B. Artyukhin, C.P. Grigoropoulos, A. Noy, O. Bakajin, Fast Mass Transport Through Sub-2-Nanometer Carbon Nanotubes, Science 312 (2006) 1034-1037.

[25] P.S. Goh, A.F. Ismail , B.C. Ng, Carbon nanotubes for desalination: Performance evaluation and current hurdles, Desalination 308 (2013) 2–14.

[26] B.J. Hinds, N. Chopra, R. Andrews, V. Gavalas, L.G. Bachas, Aligned Multiwalled Carbon Nanotube Membranes, Science 303 (2004) 62-65.

[27] S.A. Miller, V.Y. Young, C.R. Martin, Electroosmotic Flow in Template-Prepared Carbon Nanotube Membranes, J. Am. Chem. Soc. 123 (2001) 12335-12342.

[28] W. Chengwei, L. Menke, P. Shanlin, L. Hulin, Well-aligned carbon nanotube array Membrane synthesized in porous alumina template by chemical vapor deposition, Chin. Sci. Bull. 45 (2000) 1373–1376.

[29] A. Srivastava, O.N. Srivastava, S. Talapatra, R. Vajtai, P.M. Ajayan, Carbon nanotube Filters, Nat. Mater. 3 (2004) 610–614.

[30] L.F. Dumee, K. Sears, J. Schütz, N. Finn, C. Huynh, S. Hawkins, M. Duke, S. Gray, Characterization and evaluation of carbon nanotube Bucky-Papermembranes for direct contact membrane distillation, J. Membr. Sci. 351 (2010) 36–43.

[31] R. Andrews, D. Jacques, A.M. Rao, F. Derbyshire, D. Qian, X. Fan, E.C. Dickey, J. Chen, Continuous production of aligned carbon nanotubes: A step closer to commercial realization, Chem. Phys. Lett. 303 (1999) 467–474.

[32] S. Majeed, D. Fierro, K. Buhr, J. Wind, B. Du, A.B.D. Fierro, V. Abetz, Multi-walled carbon nanotubes (MWCNTs) mixed polyacrylonitrile (PAN) ultrafiltration membranes, J. Membr. Sci. 403-404 (2012) 101– 109.

[33] D.L. Arockiasamy, J. Alam, M. Alhoshan, Carbon nanotubes-blended poly(phenylene sulfone) membranes for ultrafiltration applications, Appl. Water Sci. 3 (2013) 93–103.

[34] H. Wu, B. Tang, P. Wu, Novel ultrafiltration membranes prepared from a multi-walled carbon nanotubes/polymer composite, J. Membr. Sci. 362 (2010) 374–383.

[35] P. Shah, C.N. Murthy, Studies on the porosity control of MWCNT/polysulfone composite membrane and its effect on metal removal, J. Membr. Sci. 437 (2013) 90–98.

[36] Ihsanullah, T. Laoui, A.M. Al-.Amer, A. B. Khalil, A. Abbas, M. Khraisheh, M. A. Atieh, Novel anti-microbial membrane for desalination pretreatment: A silver nanoparticle-doped carbon nanotube membrane, Desalination 376 (2015) 82-93.

[37] S.J. Oh, N. Kim, Y.T. Lee, Preparation and characterization of PVDF/TiO$_2$ organic–inorganic composite membranes for fouling resistance improvement, J. Membr. Sci. 345 (2009) 13–20.

[38] R.A. Damodar, S.J. You, H.H. Chou, Study the self cleaning, antibacterial and photo catalytic properties of TiO$_2$ entrapped PVDF membranes, J. Hazard. Mater. 72 (2009) 1321–1328.

[39] L. Yan, Y.S. Li, C.B. Xiang, S. Xianda, Effect of nano-sized Al$_2$O$_3$-particle addition on PVDF ultrafiltration membrane performance, J. Membr. Sci. 276 (2006) 162–167.

[40] F. Liu, M.R.M. Abed, K. Li, Preparation and characterization of poly(vinylidene fluoride)(PVDF) based ultrafiltration membranes using nano γ-Al$_2$O$_3$, J. Membr. Sci. 366 (2011) 97–103.

[41] A. Bottino, G. Capannelli, A. Comite, Preparation and characterization of novel porous PVDF-ZrO$_2$ composite membranes, Desalination 146 (2002) 35–40.

[42] S.P. Nunes, K.V. Peinemann, K. Ohlrogge, A. Alpers, M. Keller, A.T.N Pires, Membranes of poly(ether imide) and nano dispersed silica, J. Membr. Sci. 157 (1999) 219–226.

[43] R. A. Gandhi, K. Palanikumar, B.K. Ragunath, J. P. Davim, Role of carbon nanotubes (CNTs) in improving wear properties of polypropylene (PP) in dry sliding condition, Mater. Design 48 (2013) 52–57.

[44] R. Theravalappil , P. Svoboda, J. Vilcakova, S. Poongavalappil, P. Slobodian, D. Svobodova, A comparative study on the electrical, thermal and mechanical properties of ethylene–octene copolymer based composites with carbon fillers, Mater. Design 60 (2014) 458–467.

[45] J. Huang, D. Rodrigue, The effect of carbon nanotube orientation and content on the mechanical properties of polypropylene based composites, Mater. Design 55 (2014) 653-

663.

[46] S.A.R. Hashmi, H. C. Prasad, R. Abishera, H. N. Bhargaw, A. Naik,   Improved recovery
     stress in multi-walled-carbon-nanotubes reinforced polyurethane, Mater. Design 67 (2015)
     492–500

[47] L. Liu,   D. Y. W. Di,   H. Park,   M. Son, H. G. Hurand   H.Choi, Improved antifouling
     performance of polyethersulfone (PES) membrane via surface modification by CNTs bound
     polyelectrolyte multilayers, RSC Adv. 5 (2015) 7340-7348.

[48] F. Aviles, J.V. Cauich-Rodrıguez, L. M. Tah, A. M. Pat, R. V.Coronado, Evaluation of mild
     acid oxidation treatments for MWCNT functionalization, Carbon 4 7 (2009) 2970 –2975.

[49] V. Datsyuk, M. Kalyva, K. Papagelis, J. Parthenios, D. Tasis, A. Siokou, I. Kallitsis,, C.
     Galiotis, Chemical oxidation of multiwalled carbon nanotubes, Carbon 4 6 (2008) 833 –840.

[50] Y. L. Luo, X. P. Wei, D. Cao, R. X. Bai, F. Xu, Y. S. Chen, Polystyrene-block-poly(tert-
     butyl methacrylate)/multiwall carbon nanotube ternary conducting polymer
     nanocomposites based on compatibilizers:Preparation, characterization and vapor sensing
     applications, Mater. Design 87 (2015) 149–156.

[51] H. Li, J. Fan, X. Geng, B. Li, C. Liang, H. Wang, Y. Li, Z. Qiao, J. Kang, Alumina powder
     assisted carbon nanotubes reinforced Mg matrix composites, Mater. Design 60 (2014) 637–
     642.

[52] R. Ramesh, K. Ashok, G.M. Bhalero, S. Ponnusamy, C. Muthamizhchelvan, Synthesis
     and properties of α-Fe$_2$O$_3$ nanorods, Cryst. Res. Technol. 45 (2010) 965 – 968.

[53] N. Scharnagl, H. Buschatz, Polyacrylonitrile (PAN) membranes for ultra- and
     microfiltration, Desalination 139 (2001) 191-198.

[54] H. Wu, B. Tang, P. Wu, Novel ultrafiltration membranes prepared from a multi-walled
     carbon nanotubes/polymer composite, J. Membr. Sci. 362 (2010) 374–383.

[55] F. Patel, M.A. Baig, T. Laoui, Processing of porous alumina substrate for multilayered
     ceramic filter, Desalin. Water Treat. 35 (2011) 33–38.

[56] P. Chen, H. Xie, F. Huang, T. Huang, Y. Ding, Deformation and failure of polymer bonded
     explosives under diametric compression test, Polym. Test. 25 (2006) 333–341.

[57] Y. Ma, F. Shi, J. Ma, M. Wu, J. Zhang, C. Gao, Effect of PEG additive on the morphology
     and performance of polysulfone ultrafiltration membranes, Desalination 272(1-3) (2011)

51–58.

[58] G.D. Vilakati, E.M.V. Hoek, B.B. Mamba, Probing the mechanical and thermal properties of polysulfone membranes modified with synthetic and natural polymer additives, Polym. Test. 34 (2014) 202–210.

[59] B.P. Frank, G. Belfort, Polysaccharides and sticky membrane surfaces: critical ionic effects, J. Membr. Sci. 212 (2003) 205–212.

[60] Y.Ye, P.L. Clech, V. Chen, A.G. Fane, B. Jefferson, Fouling mechanisms of alginate solutions as model extracellular polymeric substances, Desalination 175 (2005) 7–20.

[61] K.S. Katsoufidou, D.C. Sioutopoulos, S.G. Yiantsios, A.J. Karabelas, UF membrane fouling by mixtures of humic acids and sodium alginate: Fouling mechanisms and reversibility, Desalination 264 (2010) 220-227.

[62] E. Aoustin, A.I. Schaefer, A.G. Fane, T.D. Waite, Ultrafiltration of natural organic matter, Sep. Purif. Technol. 22-23 (2001) 63–78.

[63] K. Katsoufidou, S.G. Yiantsios, A.J. Karabelas, Experimental study of ultrafiltration membrane fouling by sodium alginate and flux recovery by backwashing, J. Membr. Sci. 300 (2007) 137–146.
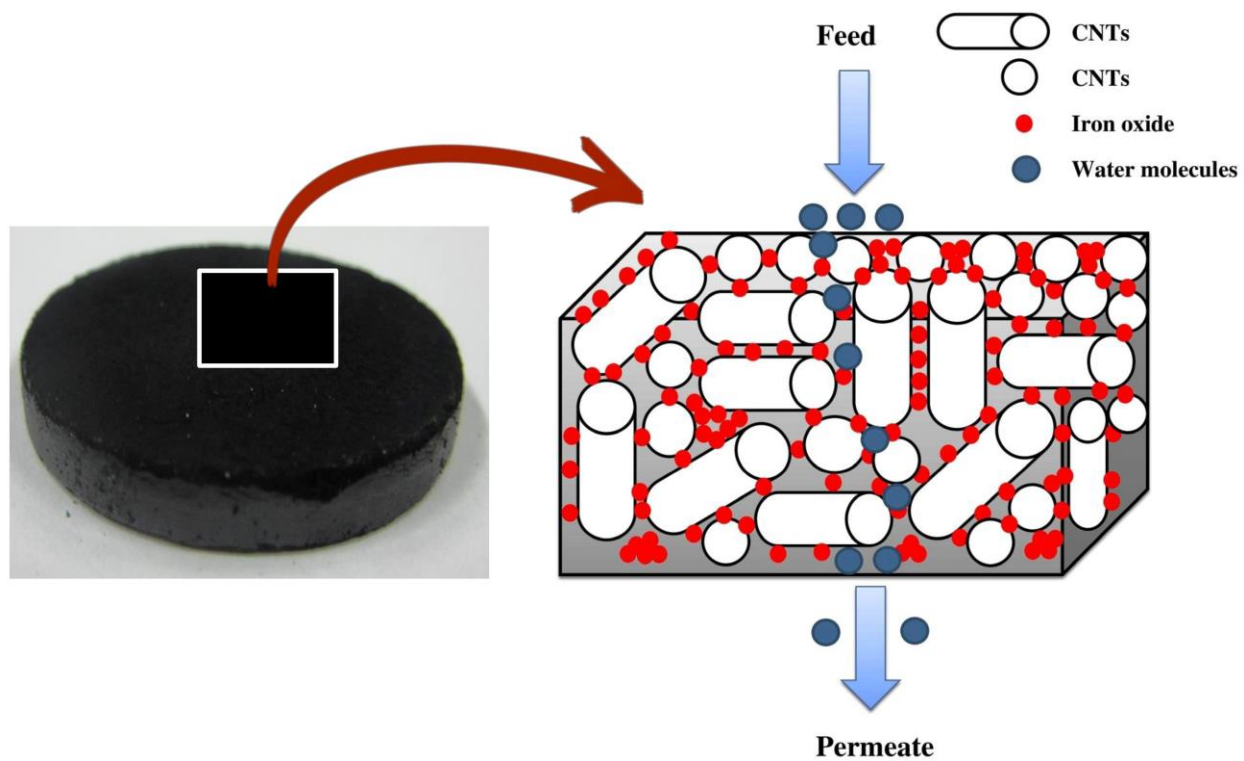
Graphical Abstract

Highlights:

- Membranes comprising of iron oxide-impregnated carbon nanotube were synthesized.

- The iron oxide nanoparticles serve as a binder to hold the nanotubes together in the matrix.

- The novel CNT membrane exhibited high water flux and strong antifouling behavior.

- The membrane characteristics were influenced by the iron oxide content.